# Cavities in Molecular Liquids and the Theory of Hydrophobic Solubilities

**Andrew Pohorille[†] and Lawrence R. Pratt*[,‡]**

*Contribution from the Department of Chemistry, University of California, Berkeley, California 94720, and the Chemical and Laser Sciences Division, Los Alamos National Laboratory, Los Alamos, New Mexico 87545.* *Received December 21, 1989*

**Abstract:** Thermal configurational data on neat liquids are used to obtain the work of formation of hard spherical cavities of atomic size in six molecular solvents: *n*-hexane, *n*-dodecane, *n*-undecyl alcohol, chloroform, carbon tetrachloride, and water. These results are used to test a recent suggestion that the differences between nonaqueous solvents and liquid water in solvation of inert gases are not principally due to the hydrogen-bonded structure of liquid water but rather to the comparatively small size of the water molecule. The frequencies of occurrence of cavities in liquid water can be meaningfully distinguished from those in the organic solvents. Liquid water has a larger fractional free volume, but that free volume is distributed in smaller packets. With respect to cavity work, water is compared to a solvent of the same molecular density and composed of hard spheres of the same size as the water molecule. That comparison indicates that the hard-sphere liquid finds more ways to configure its free volume in order to accommodate an atomic solute of substantial size and, thus, would be a more favorable solvent for inert gases. The scaled particle model of inert gas solubility in liquid water predicts cavity works 20% below the numerical data for TIP4P water at 300 K and 1.0 g/cm$^3$ for cavity radii near 2.0 Å. It is argued that the sign of this difference is just the sign that ought to be expected and that the magnitude of this difference measures structural differences between water and the directly comparable hard-sphere liquid. In conjunction with previous data, these results indicate that atomic sized cavities should be considered submacroscopic.

In recent years, applications of the scaled particle model[1,2] to studies of solubilities of inert gases in molecular liquids[3,4] have led to a suggestion that the characteristic differences between nonaqueous solvents and liquid water are not due to the structure of liquid water. Instead, it is suggested that they are due principally to the comparatively small size of the water molecule.[4] This physical picture has not been directly tested even though hydrophobic phenomena are of broad interest in colloid and materials sciences as well as in biophysical chemistry. Moreover, this is a picture that should be readily clarified by persistence in accumulating the relevant liquid structural data and attention to simple, basic issues of the theory of liquids. For these reasons, we have undertaken a study, utilizing computer experiment, of a basic feature of solubility of inert gases in molecular liquids: the likelihood of finding, at an arbitrary point in the solvent, an atomic sized cavity that could accommodate the solute.

The cavity data of the type analyzed here could, with additional work, yield predictions of the solubilities of simple atomic species in molecular solvents. This has not been done here because these data are of more immediate interest as signatures of the solvent structure which influence those solubilities. The solubility of inert gases is characteristically different in water than in common organic solvents. Therefore, the likelihood of observing a natural occurrence of a cavity of atomic dimensions might be expected to be characteristically different in liquid water than in nonassociated liquids. Despite this reasonable expectation, it has not been known with any confidence whether these signatures could be distinguished in any meaningful way using thermal configurational data obtained by computer simulation techniques with current intermolecular force models.

Since these data are simple and reflect a property of the solvent alone, they are of general use in comparing different solvents. For this reason, too, these data provide a basis for clarifying general conceptual pictures of hydrophobic effects, perhaps more effectively than specific computational results on particular solute/solvent systems.

The scaled particle model describes the cavities that might occur in a liquid by assigning a van der Waals or excluded volume to the solvent molecules and then considering the volume accessible to a spherical solute. The atomic (or extended atom) constituents of the fluid might be used to define the excluded volume. In typical applications of the scaled particle model, however, the excluded volume is treated by modeling the solvent molecules as impenetrable spheres. The predictions of the scaled particle model are sensitive to the value of the radii of those spherical exclusion volumes. The value assigned to the radius of the water molecule usually differs by nearly a factor of 2 from values assigned to organic solvents such as carbon tetrachloride. It has been noted that this difference is the dominant factor in controlling the prediction of the solubility of inert gases in water relative to organic liquids.[3,4] It was this observation that led to the suggestion that behavior characteristic of hydrophobic solvation is due principally to the small size of the water molecule and only indirectly to the hydrogen-bonded structure of liquid water.[4]

More accurately, the scaled particle model indicates that the frequency of occurrence of atomic sized cavities is low in liquid water compared to common organic solvents. Within the scaled particle model this low frequency of occurrence of cavities of substantial size follows from the assignment of a small characteristic length for the solvent structure, the radius of a water molecule. Consequently, the available interstitial holes are quite small.

Such an argument can be considered in terms of the detailed molecular structures that are encountered in typical solvents. In fact, the scaled particle model incorporates only a meager amount of the molecular structure that might differentiate water from other solvents. This point has been emphasized previously.[2] The radii assigned to molecules as different in shape as water, carbon tetrachloride, and *n*-hexane are not directly indicative of the local molecular structure of these liquids. Because a good deal is known about the local structure of carbon tetrachloride,[5-10] this liquid

[†] University of California.
[‡] Los Alamos National Laboratory.

(1) Pierotti, R. A. *J. Phys. Chem.* **1963**, *67*, 1840. Pierotti, R. A. *J. Phys. Chem.* **1985**, *69*, 281. Pierotti, R. A. *Chem. Rev.* **1976**, *76*, 717.
(2) Stillinger, F. H. *J. Soln. Chem.* **1973**, *2*, 141.
(3) Lucas, M. *J. Phys. Chem.* **1976**, *80*, 359.
(4) Lee, B. *Biopolymers* **1985**, *24*, 813. Lee, B. *J. Chem. Phys.* **1985**, *83*, 2421.
(5) Narten, A. H.; Danford, M. D.; Levy, H. A. *J. Chem. Phys.* **1967**, *46*, 4875. Narten, A. H. *J. Chem. Phys.* **1976**, *65*, 573.
(6) Egelstaff, P. A.; Page, D. I.; Powles, J. G. *Mol. Phys.* **1971**, *20*, 881.
(7) Lowden, L. J.; Chandler, D. *J. Chem. Phys.* **1974**, *61*, 5228.
(8) Steinhauser, O.; Neumann, M. *Mol. Phys.* **1980**, *40*, 115.
(9) McDonald, I. R.; Bounds, D. G.; Klein, M. L. *Mol. Phys.* **1982**, *45*, 521.
(10) Adan, F. S.; Banon, A.; Santamaria, J. *Chem. Phys. Lett.* **1984**, *107*, 475.

0002-7863/90/1512-5066$02.50/0 

can provide a simple example. At the densities of interest, neighboring $CCl_4$ molecules interlock appreciably. This interlocking is principally due to the chemical structure of the $CCl_4$ molecule and van der Waals contacts associated with the chlorine atoms. This suggests that the Cl van der Waals radii would give a more accurate indication of the size of interstitial cavities that might exist in liquid carbon tetrachloride. In this respect, it is not obvious that the molecules can be viewed accurately as impenetrable spheres with a van der Waals radius determined by typical near-neighbor C···C distances.

Similar considerations apply to the molecular structure of liquid water. Efficient packing of small molecules such as $H_2O$ molecules at a liquid density will leave rather small interstitial spaces. However, water is often thought of as a liquid of open architecture. For example, a solvent atom or molecule in a generic simple liquid near its triple point typically has between 9 to 12 near-neighbors.[11] In contrast, a $H_2O$ molecule in water near its triple point has fewer near neighbors, between 3 and 6, and these neighbors are more precisely located. This architectural openness is often emphasized in discussions of the peculiar increase in density of liquid water as it is heated at constant pressure just above its normal melting point. Again, the fidelity of an interpretation of solubility data on the basis of packing of spheres is not obvious.[12]

The research reported here has the objective of clarifying these views. During recent years, we have accumulated a data base of thermally representative configurations for an interesting range of molecular liquids. Although these data were obtained originally for other purposes,[13-16] they permit several of the comparisons that should be helpful in gaining a more accurate picture of hydrophobic solvation. Water as well as polar and nonpolar organic liquids are represented. The nonaqueous solvents include liquids of rigid and nonrigid molecules. Results for two different models of liquid water are available and in one of those cases for two different temperatures.

A simple statement of the theory that is the basis of the present analysis follows in the next section. We then note some of the methodological details associated with the analysis and present our results. These results are then discussed and compared with previous work. Finally, we present the conclusions that may be drawn from this work.

## Theory

Progress in a theoretical understanding of hydrophobic effects has been limited by lack of physical, molecular-level hypotheses that are also a natural part of the broader theory of liquids. Physical suggestions without this latter quality are not very helpful in distinguishing water from other liquids. For this reason, it is important to present here a discussion of the theoretical ideas to be tested below. In fact, the analysis in subsequent sections of this paper can be understood on the basis of a simple, general theoretical development. This discussion then serves the additional purpose of defining the quantities to be analyzed.

The discussion by Stillinger[2] may be consulted for a somewhat different perspective which, however, is closely related to the present ideas. The central result of this development is a statistical formula that provides the chemical potential $\mu_R$ of a hard-sphere solute of radius $R$ dissolved in the solvent

$$\mu_R/k_BT = \ln(\rho_R\Lambda_R^3) - \ln(\langle V_R\rangle/V) \quad (1)$$

where $V_R$ is the volume accessible to the observation particle, a hard sphere of radius $R$, and $V$ is the total volume. Here $T$ is the temperature, $k_B$ is Boltzmann's constant, $\rho_R$ is the solute density, and $\Lambda_R$ is the thermal deBroglie wavelength. The brackets in eq 1 indicate the ensemble average over configurations of the solvent unaffected by the observation particle. This result can be set in a much more general context by appealing to the potential distribution theorem.[17,18] However, we will not need that generality here. The ratio

$$p(R) = \langle V_R\rangle/V \quad (2)$$

is the fractional free volume. It takes on values between 0 and 1. Because it describes the likelihood of a successful insertion of a hard sphere of radius $R$ into the liquid at a randomly chosen point, we will refer to $p(R)$ as the insertion probability.

Now consider in more detail the case in which the van der Waals volume of the solvent is modeled by assigning an exclusion sphere to each of the interaction sites that describe the solvent molecules. The insertion probability can then be expressed as

$$p(R) = \langle\prod_{\alpha j}\{1 - \eta(R + R_\alpha - |\mathbf{r} - \mathbf{r}_{\alpha j}|)\}\rangle \quad (3)$$

The product is over all exclusion spheres, $\alpha j$ identifying the $j$th exclusion sphere of type $\alpha$ which is located at $\mathbf{r}_{\alpha j}$. The radius assigned to exclusion spheres of type $\alpha$ is $R_\alpha$. Here $\eta(z)$, the Heaviside function, is defined by

$$\eta(z) = \begin{cases} 0, & z < 0 \\ 1, & z > 0 \end{cases} \quad (4)$$

For a particular configuration and a particular point $\mathbf{r}$, the product is 1 if no overlaps occur and 0 otherwise. Therefore, eq 3 faithfully evaluates the desired quantity.

If the product of eq 3 is multiplied out and all terms with the same number of factors of $\eta(z)$ are collected, the Mayer–Montroll expansion for the present problem is obtained.[19] Succeeding terms in this expansion correspond to the possibility of the solute overlapping successively larger numbers of solvent-exclusion spheres. This is an essential ingredient of the scaled particle theory for the equation of state of the hard-sphere fluid.[20] Note, in particular, that the observation point, located at some definite position, can penetrate only a finite number of exclusion spheres. Thus, this expansion truncates at a finite number of terms. An important example is the case in which the exclusion spheres do not overlap each other. The solute can occupy only one solvent sphere at a time and the expansion terminates at the second term.

$$p(R) = 1 - \sum_\alpha \int \eta(R + R_\alpha - |\mathbf{r} - \mathbf{r}'|)\rho_\alpha(\mathbf{r}')\,d\mathbf{r}'$$
$$= 1 - \frac{4\pi}{3}\sum_\alpha (R + R_\alpha)^3\rho_\alpha \quad (5)$$

The density of exclusion spheres of type $\alpha$ is $\rho_\alpha$. This result for the fractional free volume is valid when $R + R_\alpha$ is sufficiently small that the excluded volume is a disjoint set of spherical volumes. This can be achieved by allowing $R$ to decrease sufficiently and, in particular, to take on negative values in a restricted range which ensures that the right side of eq 5 is not greater than unity. This result is an important ingredient in scaled particle theories, both the original scaled particle development for the hard-sphere fluid[20] and the scaled particle model for the solubility

(11) See, for example: Hansen, J. P.; McDonald, I. R. *Theory of Simple Liquids*; 2nd ed.; Academic Press: New York, 1986.

(12) With the available computer simulation models, the characteristic hydrophobic temperature behavior of the solubility of inert gases in simulated aqueous solutions seems to be captured faithfully only if the distance of closest approach between the solute and a water molecule is assumed to be considerably larger than the natural initial guesses. See: Swope, W. C.; Andersen, H. C. *J. Phys. Chem.* **1984**, *88*, 6548.

(13) Most of that other research is not germane to the present considerations. However, ref 14–16 give a fuller indication of the sources of some of the present data.

(14) Pohorille, A.; Burt, S. K.; MacElroy, R. D. *J. Am. Chem. Soc.* **1984**, *106*, 402.

(15) (a) Wilson. M. A.; Pohorille, A.; Pratt, L. R. *J. Phys. Chem.* **1987**, *91*. 4873. (b) Wilson, M. A.; Pohorille, A.; Pratt, L. R. *J. Chem. Phys.* **1988**, *88*, 3281.

(16) Pohorille, A.; Pratt, L. R.; LaViolette, R. A.; Wilson, M. A.; MacElroy, R. D. *J. Chem. Phys.* **1987**, *87*, 6070.

(17) Widom, B. *J. Chem. Phys.* **1963**, *39*, 2808. Widom, B. *J. Stat. Phys.* **1978**, *19*, 563. Widom, B. *J. Phys. Chem.* **1983**, *86*, 869.

(18) Jackson, J. L.; Klein, L. S. *Phys. Fluids* **1963**, *7*, 279.

(19) Mayer, J. E.; Montroll, E. *J. Chem. Phys.* **1941**, *9*, 2. See also: Stell, G. In *Studies in Statistical Mechanics*; Shlesinger, M. F., Weiss, G. H., Eds.; North-Holland: Amsterdam, 1985; Vol. XII, Chapter 6.

(20) Reiss, H. *Adv. Chem. Phys.* **1985**, *9*, 1. Reiss, H. In *Statistical Mechanics and Statistical Methods*; Landman, U., Ed.; Plenum: New York, 1977.

**Table I**

| system | calcn | molecules | $T$, K | length | configns | gridpoints |
|---|---|---|---|---|---|---|
| water (TIP4P) | MD | 343 | 300 | 100 ps | 200 | 42875 |
| water (TIP4P) | MD | 343 | 360 | 100 ps | 200 | 42875 |
| water (MCY) | MC | 343 | 300 | 100 Kpass | 200 | 42875 |
| $CCl_4$ | MC | 125 | 300 | 97 Kpass | 485 | 15625 |
| $CHCl_3$ | MC | 125 | 300 | 60 Kpass | 300 | 21875 |
| *n*-hexane | MD | 128 | 320 | 600 ps | 1200 | 27000 |
| *n*-dodecane | MD | 64 | 320 | 400 ps | 800 | 27000 |
| *n*-undecyl alcohol | MD | 64 | 320 | 350 ps | 700 | 27000 |

of inert gases in liquid water.[1,2] More generally, $p(R = 0)$ is the fractional volume accessible to a point solute and we will refer to $1 - p(R = 0)$ as the packing fraction.

In going beyond eq 5, the next term in the expansion of eq 3 can be evaluated in terms of the radial distribution function $g_{\xi\chi}(r)$ of pairs of exclusion spheres $(\xi,\chi)$ in the undisturbed solvent. We will not require the general result below because we will be particularly interested in the case where the solvent contains exclusion spheres of just one type. Therefore, we give only that special result

$$p(R) = 1 - \frac{4\pi}{3}\rho_S(R + R_S)^3 + 4\pi\rho_S^2\int_0^{2(R+R_S)} r^2 g_{SS}(r)h(r,R + R_S)\,dr \quad (6)$$

Here $R_S$ is the radius of that single type of exclusion sphere that is present at the density $\rho_S$. $h(r,\lambda)$ is the function

$$h(r,\lambda) = \left(\frac{2\pi}{3}\right)\lambda^3\left\{1 - \frac{3}{2}(r/2\lambda) + \frac{1}{2}(r/2\lambda)^3\right\} \quad (7)$$

Equation 6 is valid when $R$ is sufficiently small that the solute can penetrate no more than two solvent-exclusion spheres simultaneously.

Discussion of one further aspect of empirical scaled particle models for the aqueous solution applications is required for the analysis that follows. The variation of $p(R)$ with $R$ asymptotically for large $R$ can be anticipated on physical grounds. The variation with $R$ of the standard chemical potential, defined by

$$\Delta\mu_R \equiv \mu_R - k_BT \ln (\rho_R\Lambda_R^3) = -k_BT \ln p(R) \quad (8)$$

should describe the quasistatic work expended in altering the radius of the solute. In the aqueous solution applications, it has been customary to let the solvent van der Waals volume be associated with exclusion spheres centered on the oxygen atoms only. Thus the solvent radius $R_S$ can be identified with the oxygen atom, $R_S = R_O$. Using the notation, $\lambda = R + R_S$, we can expect that[2]

$$\Delta\mu_R \sim \frac{4\pi}{3}p\lambda^3 + 4\pi\gamma\lambda^2\left(1 - \frac{4\delta}{\lambda}\right) \quad (9)$$

Here $p$ is the pressure of the liquid. The parameters $\gamma$ and $\delta$ are considered to be conventional surface thermodynamic properties of the water liquid–vapor interface, the surface tension, and the distance between the equimolar surface and the surface of tension.[21] This identification should not be considered rigorous in this context, but it is reasonable for many solvents under standard conditions and, in particular, for water near liquid–vapor phase coexistence at low pressure.[2] The original application of scale particle methods to aqueous solutions required that the asymptotic result of eq 9 join smoothly at $R = 0$ to the low $R$ behavior described by eq 5. The requirement that $\Delta\mu_R$ be continuous and smooth at $R = 0$ constitutes two additional conditions on the coefficients of this asymptotic form. If the pressure $p$ is supplied from experiment, those conditions determine $\gamma$ and $\delta$ and the theory then predicts the limiting low-pressure solubilities of a hard sphere in liquid water.

(21) See, for example: Rowlinson, J. S.; Widom, B. *Molecular Theory of Capillarity*; Clarendon Press: Oxford, 1982; Section 2.4.

## Methods

The insertion probabilities $p(R)$ were calculated for six different liquids: *n*-hexane, *n*-dodecane, *n*-undecyl alcohol, chloroform, carbon tetrachloride, and water. Table I gives a summary of the configurational data. These configurations were obtained either by Newtonian molecular dynamics calculations or Metropolis Monte Carlo methods. The calculations on water were performed for the TIP4P[22] and the MCY[23] model. In these cases the intermolecular pair interactions were smoothly truncated as is indicated in refs 15 and 16. The interaction potential energy models for *n*-hexane, *n*-dodecane, and *n*-undecyl alcohol were those developed by Jorgensen.[24] Again, the intermolecular interactions were smoothly truncated with a cubic spline which brought the united atom site–site interactions smoothly to zero at the outer cutoff distance of 12.0 Å. The inner-spline knot was located at 11.5 Å. For carbon tetrachloride a model potential function thoroughly investigated in a Monte Carlo study of solvation of nucleic acid bases was used.[14,25] This model function was extended to include H···Cl and H···C atom interactions and employed in a Monte Carlo study of liquid chloroform.[26] All calculations used a cubic simulation volume, and periodic boundary conditions were applied in all three spatial directions. In all cases except for TIP4P water at 360 K, the calculations were carried out at the experimental normal densities for the temperature in question. For that exception the density was 1.0 g/cm$^3$.

To obtain the insertion probabilities for a particular system a grid of test points evenly spaced in the simulation cell was created. The number of gridpoints for each system is given in Table I. Then for each configuration and each gridpoint, the nearest exclusion sphere of each type was found. This permitted the determination of the radius of the largest cavity that could be inserted at the gridpoint in question for that particular configuration and for each set of solvent radii. The radii of the largest cavities that could be inserted were binned and averaged over both gridpoints and sampled configurations. This produces the probability density of the radius of the largest cavity that could be successfully inserted; that is, the probability density $p_m(R)$ with the interpretation that $p_m(R)\Delta R$ is the probability that the radius of the largest cavity which could be inserted is within $\Delta R$ about $R$. The probability for insertion of a cavity with a particular radius, $R$, is equal to the likelihood that the radius considered is less than the radius of the largest cavity that can be inserted. Thus,

$$p(R) = \int_R^\infty p_m(R')\,dR' \quad (10)$$

This relation is a slight generalization of a central ingredient of the scaled particle theories,[20] and it will arise again in the discussion below. It is worth noting here that the procedure built upon eq 10 yields a range of data for each gridpoint and each configuration. It is, therefore, more efficient than hit-or-miss trial insertion of a hard-sphere solute of fixed radius.[27]

(22) Jorgensen, W. L.; Chandrasekhar, J.; Madura, J. D.; Impey, R. W.; Klein, M. L. *J. Chem. Phys.* **1979**, *79*, 926.
(23) Matsuoka, O.; Clementi, E.; Yoshimine, M. *J. Chem. Phys.* **1976**, *64*, 1351.
(24) Jorgensen, W. L. *J. Am. Chem. Soc.* **1981**, *103*, 341.
(25) Pohorille, A.; Burt, S. K. Unpublished Monte Carlo studies of liquid $CCl_4$. In addition to ref 14, see also: Pohorille, A.; Pratt, L. R.; Burt, S. K.; MacElroy, R. D. *J. Biomol. Struct. Dyn.* **1984**, *1*, 1257.
(26) Pohorille, A.; Burt, S. K. Unpublished Monte Carlo studies of liquid $CHCl_3$. In units of the magnitude of the electron charge, the partial charges used for the carbon (C), chlorine (Cl), and hydrogen (H) atoms were respectively: $q_C = 0.2829$, $q_{Cl} = -0.1173$, and $q_H = 0.069$.
(27) This distinction is analogous to the distinction between "hit-or-miss" and "crude" Monte Carlo discussed in MONTE CARLO METHODS, by Hammersley and D. C. Handscomb (Wiley: New York, 1964). Section 5.2. "Hit-or-miss" Monte Carlo is more crude than "crude".
(28) Hsu, C. S.; Chandler, D. *Mol. Phys.* **1979**, *37*, 299.
(29) Bohm, H. J.; Ahlrichs, R. *Mol. Phys.* **1985**, *54*, 1261.

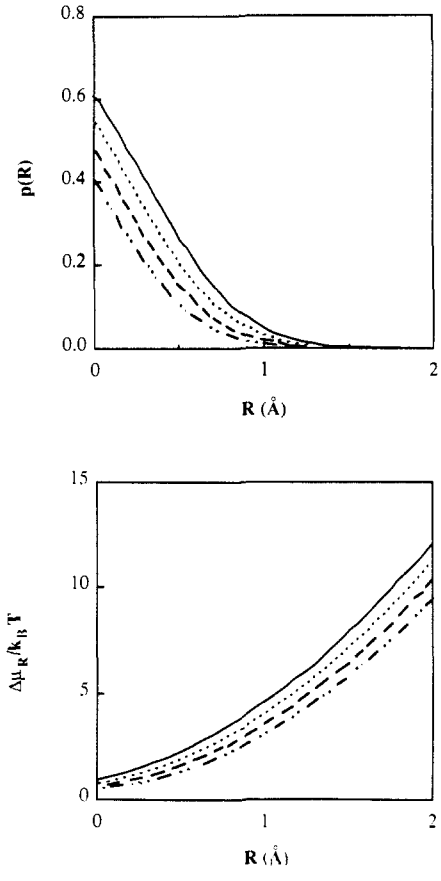


**Figure 1.** Variation of insertion probability, $p(R)$, and dimensionless cavity work, $\Delta\mu_R/k_BT$, with the van der Waals radius of chlorine for liquid carbon tetrachloride with $R_C$ = 1.54 Å. Top panel: $R_{Cl}$ = 1.55, 1.65, 1.75, 1.85 Å from top curve to bottom curve. Since $\Delta\mu_R/k_BT \equiv -\ln p(R)$ this order is reversed on the bottom panel.

Several sets of radii were considered. Assignment of van der Waals radii for many atom types is quite conventional. It may be less so for the chlorine atoms involved in the present study, so we discuss first how these radii were chosen for liquid $CCl_4$. Intermolecular Cl···Cl near-neighbors are typically separated by 3.8 Å, but the distance of closest approach for Cl···Cl pairs is about 3.4 to 3.5 Å.[5-10] The variation of our cavity results with variation of $R_{Cl}$ is shown in Figure 1. (These results also indicate that cavities nearly as large as the atoms which constitute the liquid occur with appreciable probability, i.e., nearly 1%.) In view of these results, we adopted the value $R_{Cl}$ = 1.70 Å for the van der Waals radius of the chlorine atom in the $CCl_4$ molecule.

The van der Waals radius assigned to the carbon atom is less important. We have, somewhat arbitrarily, chosen $R_C$ = 1.54 Å, but calculations with reasonable values of $R_{Cl}$ and $R_C$ = 0.0 Å produced negligible changes. The radii for the C and Cl atoms in $CCl_4$ are also reasonable for those atoms in the $CHCl_3$ molecule.[28,29] For that H atom, a value near $R_H$ = 1.0 Å is appropriate. We investigated $R_H$ = 0.95 and 1.20 Å and noted that the insertion probabilities are negligibly different for these two cases. The results for chloroform shown below used the larger value. It has become customary to treat the $H_2O$ molecule also as a single spherical exclusion volume with radius 1.35 Å centered on the oxygen atom; this custom was adopted in the results below. The methyl and methylene groups of *n*-dodecane and *n*-undecyl alcohol were all treated as united atom spherical exclusion volumes. The common and reasonable value of 1.85 Å for the van der Waals radii of the methyl and methylene groups was adopted. The hydroxyl group was also treated as a spherical extended atom centered on the oxygen atom with a van der Waals radius of 1.35 Å.

We investigated the variations of the results with changes of all the van der Waals radii within a range of ±0.2 Å. The results of Figure 1 are typical of the smooth gradation of results found when these radii are changed slightly near the values discussed.

Data on cavities with radii considerably larger than 2.0 Å were routinely collected. Our experience with the approach outlined above suggests that determination of cavity works for cavities as large as 2.3 Å in liquid water would present no special difficulties. For the hydrocarbon liquids considered here, we feel that cavity works for cavities nearly as large as 3.0 Å could be reliably obtained. Much of our discussion below is limited to cavities of considerably smaller radii so that we can inspect and compare all the data over a common range of radii for which statistical uncertainties are negligible. The method adopted here takes advantage of the homogeneity of the neat liquid and collects data throughout the sample volume. This method is, therefore, very much more efficient and precise for the present purposes than the study of the solvation of a solute actually present in the solvent.

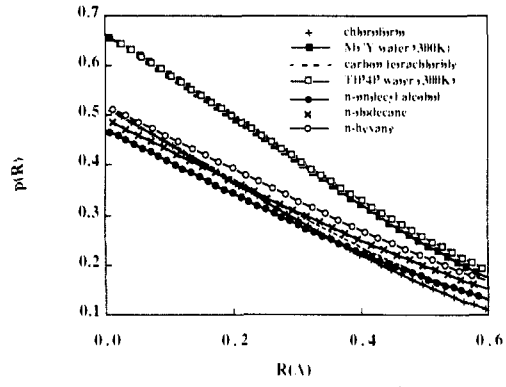


**Figure 2.** Cavity insertion probabilities for small-radius cavities in seven simulated molecular liquids. The plotting symbols identify the same liquids in each of Figures 2, 3, and 6: (+) chloroform; (■) MCY water; (---) carbon tetrachloride; (□) TIP4P water; (●) *n*-undecyl alcohol; (×) *n*-dodecane; and (○) *n*-hexane.

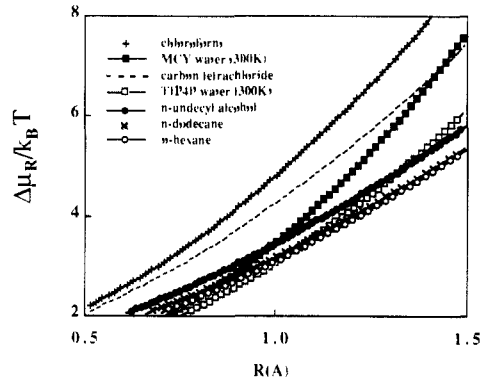


**Figure 3.** Dimensionless cavity work, $\Delta\mu_R/k_BT$, as a function of cavity radius $R$ in seven simulated molecular liquids.

## Results

Figures 2 and 3 give a composite impression of all of our results. Figure 2 shows the insertion probability $p(R)$ for all the liquids considered. These results emphasize the differences between these liquids for small cavity sizes. Figure 3 displays the cavity work $\Delta\mu_R/k_BT = -\ln p(R)$, which more clearly reveals the differences in the insertion probabilities for the larger cavity sizes where $p(R)$ is small.

The configurational data used for the different liquids considered correspond to slightly different temperatures. We anticipate that modest changes in the temperature (at constant density) of liquids considered here would engender changes in cavity insertion probabilities that are secondary to the changes seen between the different liquids studied. Therefore, we intend to consider these results principally on the basis of the differing molecular structure of these liquids. However, some checking of the size of temperature effects is warranted. Furthermore, temperature effects are often given particular attention in defining hydrophobic behavior. In order to check the size of these temperature effects, we used the data on cavity formation in TIP4P water at temperatures of 300 and 360 K at the same density, 1.0 g/cm$^3$. Figure 4 shows the changes

$$\Delta[\Delta\mu_R/k_BT] \equiv [\Delta\mu_R/k_BT]_{T=360K} - [\Delta\mu_R/k_BT]_{T=300K}$$

observed as well as the ratio of the insertion probabilities

(30) Postma, J. P.; Berendsen, H. J. C.; Haak, J. R. *Faraday Symp. Chem. Soc.* **1982**, *17*, 55.

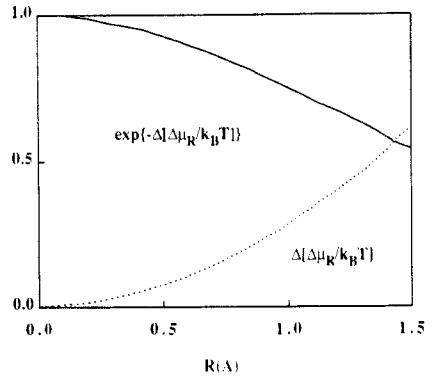


**Figure 4.** Effect of temperature on cavity formation at constant density; $\Delta[\Delta\mu_R/k_BT] \equiv [\Delta\mu_R/k_BT]_{T=360K} - [\Delta\mu_R/k_BT]_{T=300K}$ for TIP4P water with density of 1.0 g/cm$^3$.

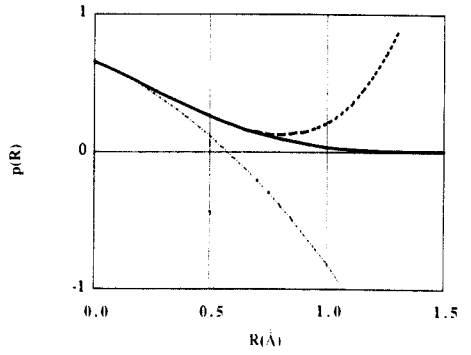


**Figure 5.** Comparison of approximate results of eqs 5 and 6 with numerical data for the TIP4P model at 300 K and 1.0 g/cm$^3$: the numerical data are the middle (solid line) curve, eq 5 is the lower (---) curve, and eq 6 is the upper (--) curve.

$\exp\{-\Delta[\Delta\mu_R/k_BT]\}$. Those results indicate that the work of cavity formation increases as the temperature increases with the density constant. The temperature differences vanish for small cavities but begin to be appreciable for the largest cavities seen. Further work which investigates the effects of density variations should be pursued in order to interpret the temperature dependence of inert gas solubilities.[12]

The $p(R)$ data (Figure 2) clearly indicate that the liquids studied fall into two categories. The results for the simulated organic liquids cluster into one group and the two water models constitute a second group. For the smaller sized cavities, the insertion probabilities are higher for the water models than for the simulated organic liquids. This means that less work is required to create a cavity of small radius in water than in the organic liquids. In view of eq 5, this can be ascribed to the fact that the packing fraction for water at 1.0 g/cm$^3$ is smaller than the packing fractions appropriate to the simulated organic liquids.

Since the results for sufficiently small cavities principally reflect the equation of state and not the detailed intermolecular structure, it is interesting to ask over what range of cavity sizes does that structure first become important. We have addressed this question in the case of TIP4P water by evaluating the approximate results of eqs 5 and 6 and comparing them with the numerical data. As with the numerical data, we took $R_H = 0.0$ Å and $R_O = R_S = 1.35$ Å. The comparison is shown in Figure 5. We conclude that the small-cavity approximation, eq 5, is accurate for $R \leq 0.2$ Å and details of molecular structure are unimportant in that range. Inclusion of the last term of eq 6 extends the range of validity to $R \leq 0.7$ Å. In this larger range the only aspect of molecular structure that influences the numerical data is the pair distribution of oxygen atoms. If the value $2 \times 1.35$ Å is taken as a distance of closest approach for the solvent oxygen atoms, then triple overlaps can occur first at a solute radius of $(2/\sqrt{3} - 1)1.35$ Å $\approx 0.2$ Å. This is smaller than 0.7 Å. It would be natural to explain part of the difference by noting that the most compact solvent triples, those that form isosceles triangles of side $2 \times 1.35$ Å, or

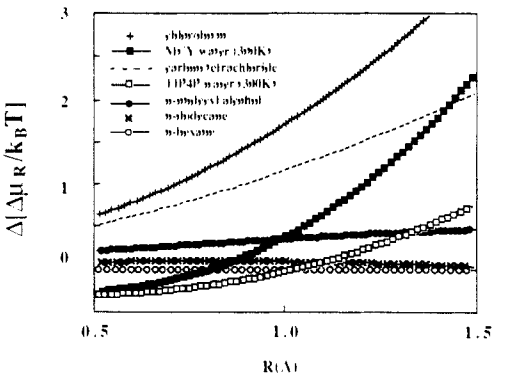


**Figure 6.** Dimensionless cavity work as a function of cavity radius in seven simulated molecular liquids relative to the computed value for *n*-hexane at that radius: $\Delta[\Delta\mu_R/k_BT] \equiv \Delta\mu_R/k_BT - [\Delta\mu_R/k_BT]_{n\text{-hexane}}$.

nearly so, are rather unlikely in liquid water.

In view of the results shown by Figure 2 and solubility experiments, the curves describing the dimensionless cavity works $\Delta\mu_R/k_BT$ for the two different categories of liquids should cross as $R$ increases. This is based on the expectation that the solubilities of atomic-sized, inert, rigid spheres should be lower in water than in typical organic liquids. The cavity work data shown in Figure 3 agree with this idea. In these results, the curves for the model water liquids seem to be similar to each other in displaying stronger curvature than the results for the organic liquids. This distinction follows from the idea that the work of formation of cavities in water should exceed those for nonaqueous liquids when the cavities are sufficiently large—even though the cavity work for small cavities is lower in water than for the other cases.

This curvature difference can be looked for more closely in Figure 6, which displays all the cavity works referenced to the value computed for *n*-hexane. More quantitatively, these curvatures were further analyzed by fitting the numerical data in the range 0.5 Å $< R <$ 1.5 Å (the range shown in Figure 3) to a model form suggested by the asymptotic behavior of eq 9:

$$\Delta\mu_R = \frac{4\pi}{3}p\lambda^3 + 4\pi\gamma\lambda^2\left(1 - \frac{4\delta}{\lambda}\right) \qquad (11)$$

with $\lambda = (R + R_S)$. The parameters of the fit are $(p, \gamma, \delta, R_S)$. The parameter $R_S$ is thus a single empirical length parameter for each liquid even for the organic liquids which involved exclusion spheres of several different sizes. Since the model depends nonlinerly on these parameters, the fitting was implemented in two steps. First the data were fit to a polynomial model

$$\Delta\mu_R/k_BT = \sum_{j=0}^{3} c_j R^j \qquad (12)$$

by a straightforward linear least-squares procedure. Expression of the coefficients $c_j$ in terms of the model parameters shows that $R_S$ must satisfy the cubic equation

$$0 = \sum_{j=0}^{3} c_j(-R_S)^j \qquad (13)$$

This can be solved analytically as the second step in the fitting procedure. Extraction of the remaining parameters from the $c_j$ and $R_S$ is then trivial.

The fitted models obtained in this way always provided a very close description of the data and in all cases the cubic eq 13 was found to have exactly one real root. Those fitted forms support the hypothesis that the results for the water models can be distinguished from those for the other liquids considered on the basis of the curvature: The fitted parameter $p$ for the water results was significantly larger than that for the other cases and the curves for the water models are, therefore, more strongly cubic. However, the fitting of the macroscopic form eq 11 to the data for atomic-sized cavities is problematic. In particular, the numerical data show a gentle and monotonic variation that can be reasonably fit by a variety of functional models or, within one functional model,

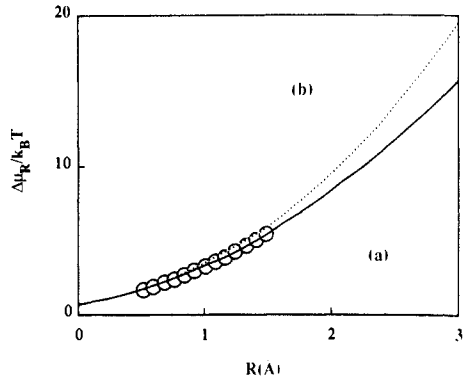


**Figure 7.** Two models fitted to the numerical data $\Delta\mu_R/k_BT$ for *n*-dodecane. The data utilized for this fit are the same as those shown in Figure 4, which spans the radius range 0.5 Å ≤ $R$ ≤ 1.5 Å. The lower curve (a) is the unconstrained fit of the model eq 11 to the data. The fitted parameters ($p,\gamma,\delta,R_S$) are all found to have negative values and, in particular, $p/k_BT = -0.012$ Å$^{-3}$. The upper curve (b) is the fit to the model eq 11 with the additional constraint that $p/k_BT = 0.03$ Å$^{-3}$, an arbitrary, positive value of reasonable size.

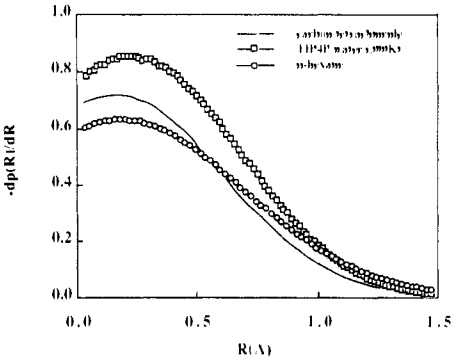


**Figure 8.** The probability density, $-dp(R)/dR$, that the maximum size sphere that could be implanted would have radius $R$, plotted over the restricted range (0.0, 1.5 Å).

by a significant range of parameters. Therefore, the parameters produced by such a fit are not sharply defined by the data. In fact, the values found for the fitted parameters were unanticipated in several respects. In the first place, for the water models the parameter $p$ was positive and the value of that parameter was higher than the known pressures of those liquids by factors between $10^2$ and $10^3$. For each of the five simulated organic liquids, on the other hand, the fitted parameter $p$ was *negative* and small in absolute value compared to the water cases. Because of the small size of $p$ for the organic liquids, fitting of the data to a model with a constrained positive value of $p$, small in magnitude compared to the values found for the water models, produced nearly as satisfactory a description of the data as did the unconstrained model. Figure 7 illustrates the distinction between the unconstrained and constrained fit to the data for *n*-dodecane. When the fitted value of $p$ was negative, it was always found that the value of $R_S$ was also negative because the cavity work data depict an increasing function of radius in the range of our observations.

The comparison shown in Figure 7 between the cavity work data over a limited range of cavity sizes and models fitted to that data raises several points that can be addressed here. It might be queried whether it is reasonable to fit a model of macroscopic form to cavity works for cavities of such small size. Such a question should be resolved ultimately by just the type of comparison shown in Figure 7. However, we can note the following facts: First, the scaled particle model being examined in this work assumes just such a fitting of a macroscopic form to results for point solutes ($R = 0$). Second, the two fitted models shown in Figure 7 might be further distinguished by utilizing data for a larger range of cavity sizes. These data for *n*-dodecane were not used earlier to avoid confusion from comparison of the results for different liquids over different ranges of cavity sizes. However, we have found that the qualitative aspects of the unconstrained fitting, including negative values of the parameter $p$, do not change when all of our data are used. In particular, the unconstrained fit—curve a of Figure 7—persists in providing a much more faithful description of our data even when results for substantially larger cavities are included in the comparison. Third, the thermodynamic pressures predicted by the MCY model[31] and, to a much lesser degree, the TIP4P model[32] under the present conditions are higher than the experimental value for water under standard conditions.

The values obtained for the parameter $\gamma$ were similarly unexpected: $\gamma$ was always assigned a *negative* value by the fitting described above. This is true even for the model water liquids where the fitted value of $p$ was positive. Two facts are relevant to this observation. First, $\gamma$ is most straightforwardly considered as a surface free energy associated with a wall or boundary of constraint. If $\gamma$ is not interpreted as an interfacial tension then it is not required that $\gamma$ take only positive values. Second, the tension of the liquid–vapor interface of TIP4P water is higher than the experimental value for water.[15] Therefore, even if the interpretation of $\gamma$ as an interfacial tension is insisted upon, the value assigned to $\gamma$ cannot be expected to be precisely the experimental value for the water liquid–vapor interface.

## Discussion

The results above should be used as a signature with which to distinguish solvents that ought to behave quite differently as media for solvation of small inert molecules. One solvent property with a direct influence on solvation is the density. The density of liquid water near standard conditions is a manifestation of the characteristic hydrogen-bonded structure of the fluid. This is particularly noticeable in the density increase with increasing temperature at constant pressure of the liquid just above the normal melting point. The fractional free volume will change in a nonmonotone fashion with temperature near 4 °C, the temperature of maximum density at atmospheric pressure. This structural aspect of hydrophobic solubility is faithfully incorporated into scaled particle models.

Of the various quantities studied here, the conventional fractional free volume $p(R = 0)$ reflects the solvent density most directly. Water near standard conditions has a greater fractional free volume than do the other solvents considered. However, because of the small size of the water molecule, that net fractional free volume is distributed in smaller packets in liquid water than in the other cases considered. Thus, the volume accessible to hard-sphere solute of substantial size is smaller in water than in simple hydrocarbon liquids. This is true despite the fact that the interstitial pockets in, for example, liquid *n*-hexane are not those characteristic of a fluid of hard spheres of radius 2.7–3.0 Å. The interstitial cavities in a liquid such as *n*-hexane should be considered on the length scale associated with the van der Waals radius of the methyl and methylene groups with radii of approximately 1.85 Å.

The idea that the free volume might be distributed in smaller or larger units can be simply checked with the data above. In view of eq 10, $-dp(R)$ can be interpreted as the probability that the largest sphere that could be implanted would have radius $R$.[33]

(31) Owicki, J. C.; Scheraga, H. A. *J. Am. Chem. Soc.* **1977**, *99*, 7403. Impey, R. W.; Madden, P. A.; McDonald, I. R. *Mol. Phys.* **1982**, *46*, 513. Kataoka, Y. *J. Chem. Phys.* **1987**, *87*, 589.

(32) Ferrario, M.; Tani, A. *Chem. Phys. Lett.* **1985**, *121*, 182.

(33) If the solvent contains exclusion spheres of one type only, having radius $R_S$, then $p_m(R)$ can be identified with the probability density $p_{nn}(R)$ of the distance to the nearest neighbor from an arbitrary point in the liquid, according to the relation $p_m(R) = p_{nn}(R + R_S)$. The normalization of this latter quantity, $\int_0^\infty p_{nn}(R)\,dR = 1$, asserts that the distance to the nearest neighbor from any given point is surely within (0, ∞). Since $p_m(R - R_S) = p_{nn}(R)$, this relation suggests that $p_m(R)$ should be defined for $R$ ranging through negative values also. This is indeed rather natural, since, for many points of any particular configuration, a negative value of $R$ would be required for a hard-sphere solute to be implanted. This interpretation therefore emphasizes that Figure 8 shows only part of the full range of these normalized functions.

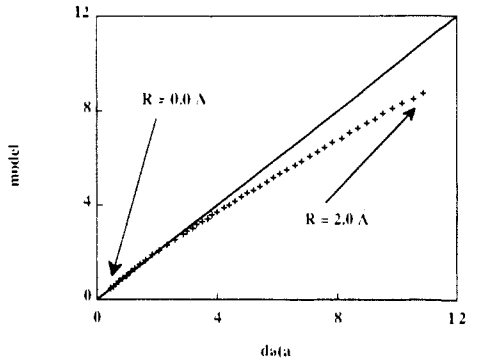


**Figure 9.** Comparison of the cavity work, $\Delta\mu_R/k_BT$, predicted by the scaled particle model (ordinate) with the cavity work observed for the TIP4P water at 300 K and 1.0 g/cm$^3$ (abscissa).

As far as they have been investigated, these distribution functions are unimodal. We will adopt the terminology that the radius corresponding to the maximum of the probability densities is the "most probable value" for the radius of largest cavity that could be inserted. Figure 8 shows the distribution functions $-dp(R)$ for three cases: TIP4P water at 300 K, *n*-hexane, and $CCl_4$. The most probable values for the largest cavity that could be inserted lie between 0.2 and 0.4 Å. However, the maximum is higher and the peak is slightly sharper for the water case than the others. This means, in the first place, that the most probable (small) cavities are more probable in water than in the other liquids. In the second place, these small cavities are somewhat more sharply defined in water than in the other liquids, particularly in view of the normalization of these distributions.[33] These distinctions are the more striking because liquid water provides more free volume than do the other solvents, as evidenced by the $p(R = 0)$ values. However, this point is consistent with preceding results such as those shown in Figure 6: Considering the comparison with the hydrocarbon liquids, small cavities, $R \ll 1.0$ Å, are more easily inserted into water. But larger cavities, $R \gg 1.0$ Å, are more easily inserted into the nonaqueous medium.

The comparison of the frequency of occurrence of cavities of various sizes might be sharpened by considering a solvent of precisely the same fractional free volume $p(R = 0)$ as water. A liquid composed of hard spheres of radius 1.35 Å and of the same density provides such a solvent. Previous calculations indicate that the solubility of a hard sphere of radius 1.35 Å is lower in water than in a solvent of the same density composed of hard spheres of the same size.[34a] On the basis of those results, we conclude that the hard-sphere solvent finds more ways to configure this free volume into packets of a sufficiently large size to accommodate the solute. This comparison suggests again that liquid water distributes its free volume in smaller packets than do natural reference solvents. In this case that difference reflects only structural differences between the two solvents.

That comparison can be further strengthened and the role of solvent structure further clarified simply by comparing the prediction of the scaled particle model with the numerical data obtained here for liquid water. The reason for this is that the scaled particle theory was created to describe the hard-sphere fluid. The success of the scaled particle theory in that case is associated with a successful account of the structural properties of the hard-sphere solvent in so far as those structural properties influence solubilities and the equation of state. The primitive scaled particle model for solubilities of gases in liquid water is, therefore, most physically interpreted as predicting the cavity work for a solvent composed of hard spheres of the same size as the water molecule, which also happens to have the same density and equation of state as does liquid water. Thus the errors in the scaled particle model can be ascribed to the differences in the structural characteristics between the hard-sphere solvent and liquid water.

The desired comparison of the predictions of the scaled particle model with the present data for TIP4P water at 300 K is given in Figure 9. That graph shows that the cavity work predicted by the scaled particle model is significantly below the numerical data for the larger cavities. A previous comparison[34b,35] revealed that it is also lower than the predictions of more sophisticated theories for the same quantities. The difference shown in Figure 9 is consistent with the expectation that the solubility of inert atomic solutes should be lower in water than that in a comparable simple liquid. This comparison, therefore, also suggests that the hard-sphere solvent finds more ways to configure this free volume into packets of sufficiently large size to accommodate the solute.

### Comparison with Previous Work

The arguments above lead to the view that the differences shown in Figure 9 are just the type of differences that ought to be anticipated. However, those expectations appear to differ in several respects from conclusions that were drawn on the basis of an especially helpful previous study,[30] which we will refer to as PBH. Here we discuss the differences between those calculations that must be considered in understanding the differences between the conclusions.

The PBH study investigated the work of formation of soft-sphere cavities in another model of liquid water, the SPC model. A soft-sphere cavity was described by an inverse-12th-power repulsion between the cavity center and the oxygen nuclei of the solvent. Cavities of radius as large as 2.7 Å, approximately, were considered. It was concluded that the scaled particle model was essentially exact for practical purposes. In this model it was assumed that $p = 0$. The value $R_O = R_S = 1.4375$ Å was used. The coefficient of the $\lambda^2$ term then implied a value of the parameter $\gamma$, which differed by about 5% from the experimental value of the tension of the liquid–vapor interface of water at 305 K. The maximum value of the radial oxygen density about the cavity center oscillated with increasing cavity radius.

The most important difference between the PBH comparison and present work is associated with the value of $R_O$. This parameter is not involved in obtaining the numerical data for the soft-sphere cavities, and it plays the role of an adjustable parameter of the fit in the PBH comparison. PBH noted that the value used there, $R_O = 1.4375$ Å, was significantly larger than the most popular values. For each configuration of the solvent, the fractional free volume $p(R)$ will increase if $R_O$ is decreased and, therefore, reduction of $R_O$ will decrease the cavity work. Thus, the PBH results for the scaled particle model would change in the direction toward the present scaled particle results if $R_O$ were to be decreased toward the value of 1.35 Å required for our comparison. Explicit calculations show that the scaled particle results used by PBH will decrease by about 25%, for cavities with radii near $R = 2.0$ Å. This ambiguity of comparison does not arise in the present work. Here hard cavities are intrinsic both to the numerical studies and to the scaled particle model results. In particular, a definite value of $R_O$ is uniquely associated with each $p(R)$ function obtained from the simulation data.

An additional, but smaller, decrease in the appropriate scaled particle model results will arise from the soft character of the cavities studied by PBH. The cavity radius $R$ utilized by PBH for their comparison would be considered the optimal, or WCA, radius if the density of the solvent were 0.[36,37] The optimal radius is expected to be a decreasing function of solvent density. Thus, the most appropriate cavity radius at the solvent density of the calculation will be somewhat smaller than that used in PBH. It is reasonable to expect that this could be responsible for a further decrease of 2–4% in the scaled particle model results that provide the more appropriate comparison. Again, it must be emphasized that this ambiguity of comparison does not arise in the work reported here.

This discussion suggests that, for cavity radii near $R = 2.0$ Å, an accumulated reduction of 20–30% in the scaled particle results

(34) Pratt, L. R.; Chandler, D. *J. Chem. Phys.* **1977**, *67*, 3683; (a) see the results of Section II.C. and Table I; (b) Figure 13 of this reference and the supporting discussion.
(35) Pratt, L. R. *Annu. Rev. Phys. Chem.* **1985**, *36*, 433.
(36) See, for example, ref 11, Section 6.3.
(37) Chandler, D.; Weeks, J. D.; Andersen, H. C. *Science* **1983**, *220*, 787.

used by PBH is justified. This encourages us to suppose that a detailed analysis of the PBH data would support the same conclusion that we have arrived at here: when identical quantities are compared, the scaled particle model will predict cavity works below the numerically exact results for liquid water. We expect the difference to be appreciable for cavities of atomic size and we argue that this difference should be interpreted as the influence of the differing structure of water and the hard-sphere liquid.

This conclusion does not negate the potential practical utility of the comparison presented by PBH. That comparison showed that a simple empirical adjustment of $R_0$ could compensate for the structural peculiarities of liquid water that are not directly built into the scaled particle model. In contrast, the objective of this work is to test and refine a recent hypothesis regarding the molecular mechanism leading to hydrophobic behavior of solubilities.

In the process of checking the results obtained from approximate integral equation theories of aqueous solutions, Tanaka[38] also produced data on the cavity insertion probability, $p(R)$. The data presented in that study were neither characterized nor analyzed in sufficient detail for us to use them unambiguously. Therefore, the comparison of those data with the results and interpretations of the present study is not very conclusive. It appears that Tanaka's cavity data on liquid water are consistent with results of this work. It is, however, less clear how his data on Lennard-Jones liquid impact the present conclusions.

We next consider the value of $\gamma$ quoted by PBH. The discussion above suggests that a significant range of values for $\gamma$ will still permit a reasonable modeling of the numerical data. In particular, although the value of the liquid–vapor interfacial tension for the SPC model is not known, an alternative value (the experimental thermodynamic tension of the liquid–vapor interface of water) can provide a reasonable description of the SPC data. A similar possibility has been verified explicitly for our data. We have fitted the scaled particle model (with $p = 0$) to our data by treating $R_S$ as an adjustable parameter, $\tilde{R}_S$, for a nonlinear least-squares treatment. This procedure produces reasonably faithful descriptions of the data although of lower quality than the more flexible fitting procedures discussed above. The value $\tilde{R}_S$ obtained by this fitting is typically significantly larger than the value of 1.35 Å that is the solvent radius for these data. $\tilde{R}_S$ took values between 1.38 and 1.40 Å depending on whether the data for larger cavities were arbitrarily assigned an enhanced weight. If the smaller cavity data were preferentially weighted, $\tilde{R}_S$ tended downwards toward the value of 1.35 Å. This reflects the fact that the scaled particle model is correct for sufficiently small cavities. Conversely, if larger cavity data were given more significance, larger values of $\tilde{R}_S$ were produced. If these values were used in the scaled particle model for the $\gamma$ parameter, the value obtained for $\gamma$ is in the range of 60 to 64 dyn/cm, which is close to the value of the experimental tension to the liquid–vapor interface of water. However, in this case it is separately known that the surface tension of the TIP4P model of water is too high by approximately a factor of 2.[15]

The preceding discussion suggests that the cavities considered here and by PBH are quite submacroscopic. The PBH results also can be examined for direct aspects of macroscopic behavior, in particular, by studying the radial distribution of oxygen density about the cavity center. For that purpose, it is useful to recall the physical arguments that might justify the comparison of $\gamma$ with the thermodynamic tension of the water liquid–vapor interface.[2] Those arguments start from the expectation that liquid water should not wet a wall that exerts a simple repulsive force on the water molecules. When the cavity radius increases sufficiently, the cavity surface can be considered as locally planar. Provided that the pressure is not high, the liquid is then expected to pull away from such a cavity surface and the intervening space is expected to be filled at rather low density. That low-density material will be more similar to a vapor phase than to the liquid phase, which occupies regions far from the cavity surface. Then the qualitative behavior of the radial density of oxygen atoms is easy to imagine. It starts at a low value near the cavity surface and makes a smooth transition, reminiscent of an interfacial density profile, to a higher density at a molecularly large distance from the cavity surface. Molecular scale structural oscillations are likely to be confined to the region near the cavity surface and to be small in amplitude compared to the major density variations associated with the transition to the higher (liquid) value of the density. Then the parameter $\gamma$ describes the additional free energy associated with density inhomogeneities much like those encountered within an interfacial density profile. This description is reasonable for thermodynamic states of low pressure, but a more general justification can be expected to be complicated. The PBH results for the radial distribution of oxygen atoms about the cavity are not at all similar to the macroscopic quantities depicted by this argument. Therefore, the PBH radial distribution results indicate that these cavities are decidedly submacroscopic as judged by examination of the oxygen density near the cavity surface.

## Conclusions

Works of formation for spherical cavities of nearly atomic size are readily obtained from thermal configurational data on neat liquids. Those results for liquid water are easily distinguished from similar data for typical organic solvents. Liquid water has a larger fractional free volume than do the organic solvents, but that free volume is distributed in smaller packets.

Compared with a solvent composed of hard spheres of the same size and of the same density, water is the less favorable solvent for inert atomic solutes. Therefore, even though the fractional free volume is the same and the sizes of typical interstitial holes are about the same, the hard-sphere liquid finds more ways to configure its free volume in order to accommodate an atomic solute of substantial size. This is an effect associated with structural differences between liquid water and the hard-sphere liquid and not merely a consequence of comparative differences in sizes or densities of the solvent molecules.

This latter conclusion was supported by providing a physical interpretation for the scaled particle model and comparing the predictions of that model with the numerical data. Since hard cavities were studied consistently, that comparison does not suffer from ambiguities in identification of the appropriate cavity radii. The scaled particle model predicts cavity works below the numerical data for TIP4P water by about 20% at 300 K for cavity radii near $R = 2.0$ Å.

Use of the macroscopic form adopted for these cavity works by the scaled particle model together with the numerical data for radii $R < 1.5$ Å in order to arrive at estimates of macroscopic thermodynamic parameters, such as the pressure, is likely to be incorrect even in the *sign* of the desired quantity. From this point of view these cavities are decidedly submacroscopic. Other results[30] suggest that for substantially larger cavities the cavity work should, with increasing cavity radius, display step-like oscillations of miniscule amplitude superimposed upon an increasing function. These oscillations also should be interpreted as structural effects associated with the molecular (or submacroscopic) scale of the cavities of interest in solubility calculations.

Increasingly, there are indications that the prominence of characteristic hydrophobic behavior depends particularly on the size of the dissolved components considered.[12,30,35] The crossover as a function of cavity radii observed here for the cavity works in water and nonaqueous solutions provides additional information on this issue. In addition, previous work has shown that the solvent hydrogen bonding patterns for water near a flat surface are different from those for water in the bulk liquid, or for water near inert gas solutes.[2,15a,39] It is, therefore, interesting and important to investigate the solvation of increasingly larger cavities with the objective of describing the switch to the hydrogen-bonding pattern characteristic of flat surfaces. The present calculations, however,

(38) Tanaka, H. *J. Chem. Phys.* **1987**, *86*, 1512.

(39) Lee, C. Y.; McCammon, J. A.; Rossky, P. J. *J. Chem. Phys.* **1984**, *80*, 4448.

did not obtain work of formation results for cavities substantially larger than the solvent molecules, and that constitutes the chief limitation on the conclusions that are drawn here. Calculations of cavity works for much larger cavities will require alternative methods.

**Acknowledgment.** We thank Michael A. Wilson for help in acquisition of some of the data. This work was supported in part by NASA-Ames-UC Berkeley Intergovernmental Personnel Exchange Agreement NCA-2 315 and by the Numerical Aerodynamics Simulation (NAS) program.

# Photoinduced Electron Transfer in Self-Associated Complexes of Several Uroporphyrins and Cytochrome *c*

**J. S. Zhou, E. S. V. Granada, N. B. Leontis, and M. A. J. Rodgers***

*Contribution from the Center for Photochemical Sciences, Bowling Green State University, Bowling Green, Ohio 43403.* *Received November 13, 1989*

**Abstract:** Photoinduced electron transfer between cytochrome *c* and free base and metallouroporphyrin (Up, MUp) has been studied. Difference absorption spectrophotometry showed that the electrostatic interactions between Up and cytc(III) result in their forming a self-associated 1:1 complex in the ground state with a binding constant that depends upon the ionic strength. In the complex, the photoexcited uroporphyrin singlet state was quenched through a static interaction with the protein. Even under the most favorable quenching conditions, i.e., when all porphyrin was complexed, residual fluorescence was noted. More significantly the excited singlet state of the complex was shown to undergo small, but significant, intersystem crossing. These triplet states rapidly underwent an electron-transfer process that yielded transiently the Fe(II) form of the protein. This is the first observation of such a process from a porphyrin/cytochrome self-association complex. Both the rates of bimolecular electron transfer between uncomplexed partners and intramolecular electron transfer from the uroporphyrin triplet to cytochrome *c*, as well as the thermal intramolecular back-reaction, have been measured by transient kinetic spectroscopy. The rate constants of intramolecular electron transfer for zinc uroporphyrin/cytochrome *c* and zinc cytochrome *c*/ferriuroporphyrin have been also determined. These three couples allow us to estimate approximately the reorganization energy $\lambda$ in the semiclassical electron-transfer theory.

It is now well-known that biological energy is channeled through the photosynthetic and mitochondrial respiratory chain via electron-transfer reactions.[1-5] This has stimulated a variety of studies, especially on fixed-site electron transfer in proteins, in an attempt to understand long-range electron-transfer reactions in biological systems. In recent years, mitochondrial cytochrome *c* has been one of the proteins most widely used as the study system,[6] since it is well characterized in terms of both primary and tertiary structure and since X-ray crystallographic structures are available for a number of native cytochrome *c* systems, thereby facilitating model building.[7] The approaches applied by a number of research groups to fix electron-transfer reaction centers at given distances in cytochrome *c* systems are either to covalently bond a donor and/or acceptor residue to specified sites on the cytochrome *c* surface[8-14] or to rely on electrostatic self-association between cytochrome *c* and its partner.[15-22]

On the basis of these concepts, we decided to study cytochrome *c*, which has six cationic lysine residues at its surface near the solvent-exposed heme site, and as redox partner use uroporphyrin, which has eight carboxylate residues on short side chains disposed around the periphery. Our hypothesis was that this pair would form an electrostatic self-associated complex in aqueous solution that could perhaps be induced to undergo electron transfer when the porphyrin was excited into its triplet state. This resembles the system employed by Cho et al.[23] who used cytochrome *c*

(1) Chance, B., DeVault, D. C., Frauenfelder, H., Marcus, R. A., Schrieffer, J. R., Sutin, N., Eds. *Tunneling in Biological Systems*; Academic Press: New York, 1979.
(2) Hatefi, Y. *Annu. Rev. Biochem.* **1985**, *54*, 1015.
(3) Dixit, B. P. S. N.; Vanderkooi, J. M. *Curr. Top. Bioenerg.* **1984**, *13*, 159.
(4) Michel-Beyerle, M. E., Ed. *Antennas and Reaction Centers of Photo-Synthetic: Bacteria*; Springer-Verlag: Berlin, 1985.
(5) Govindjee, Ed. *Photosynthesis. Energy Conversion by Plants and Bacteria*; Academic Press: New York, 1982; Vol. I.
(6) Pielak, G. J.; Concar, D. W.; Moor, G. R.; Williams, R. J. P. *Protein Eng.* **1987**, *1*, 83-88.
(7) Takano, T.; Dickerson, R. E. *J. Mol. Biol.* **1981**, *153*, 79-94. Takano, T.; Dickerson, R. E. *J. Mol. Biol.* **1981**, *153*, 95-115. Ochi, H.; Hata, Y.; Tanaka, N.; Kakudo, M.; Sakurai, T.; Aihara, S.; Morita, Y. *J. Mol. Biol.* **1983**, *166*, 407-418.
(8) Crutchley, R. J.; Ellis, W. R.; Gray, H. B. *J. Am. Chem. Soc.* **1985**, *107*, 5092-5094.
(9) Mayo, S. L.; Ellis, W. R.; Crutchley, R. J.; Gray, H. B. *Science* **1986**, *233*, 948-952.
(10) Bechtold, R.; Gardineer, M. B.; Kazmi, A.; Van Hemelryck, B.; Isied, S. S. *J. Phys. Chem.* **1986**, *90*, 3800-3804.
(11) Bechtold, R.; Kuehn, C.; Lepre, C.; Isied, S. S. *Nature* **1986**, *322*, 286-288.
(12) Elias, H.; Chou, M. H.; Winkler, J. R. *J. Am. Chem. Soc.* *110*, **1988**, 429-434.
(13) Conrad, D. W.; Scott, R. A. *J. Am. Chem. Soc.* **1989**, *111*, 3461-3463.
(14) Meade, T. J.; Gray, H. B.; Winkler, J. R. *J. Am. Chem. Soc.* **1989**, *111*, 4353-4356.
(15) Ho, P. S.; Sutoris, C.; Liang, N.; Maragoliash, E.; Hoffman, B. M. *J. Am. Chem. Soc.* **1985**, *107*, 1070-1071.
(16) Cheung, E.; Taylor, K.; Kornblatt, J. A.; English, A. M.; McLendon, G.; Miller, J. R. *Proc. Natl. Acad. Sci. U.S.A.* **1986**, *83*, 1330-1333.
(17) Liang, N.; Kang, C. H.; Ho, P. S.; Maragoliash, E.; Hoffman, B. M. *J. Am. Chem. Soc.* **1986**, *108*, 4665-4566.
(18) McLendon, G.; Miller J. R. *J. Am. Chem. Soc.* **1985**, *107*, 7811-7816.
(19) Conklin, K. T.; McLendon, G. *J. Am. Chem. Soc.* **1988**, *110*, 3345-3350.
(20) Hazzard, J. T.; Poulos, T. L.; Tollin, G. *Biochemistry* **1987**, *26*, 2836-2848.
(21) Hazzard, J. T.; McLendon, G.; Cusanovich, M. A.; Tollin, G. *Biochem. Biophys. Res. Commun.* **1988**, *151*, 429-434.
(22) Cheddar, G.; Meyer, T. E.; Cusanovich, M. A.; Stout, C. D.; Tollin, G. *Biochemistry* **1989**, *28*, 6318-6322.

0002-7863/90/1512-5074$02.50/0 